Journal of The Electrochemical Society, **151** (11) A1977-A1988 (2004)
0013-4651/2004/151(11)/A1977/12/$7.00 © The Electrochemical Society, Inc.

A Mathematical Model for the Lithium-Ion Negative Electrode Solid Electrolyte Interphase

John Christensen*,z and John Newman**

Department of Chemical Engineering, University of California, Berkeley, California 94720, USA

The passivating solid electrolyte interphase (SEI) layer forms at the surface of the negative-electrode active material in lithium-ion cells. A continuum-scale mathematical model has been developed to simulate the growth of the SEI and transport of lithium and electrons through the film. The model is used to estimate the film growth rate, film resistance, and irreversible capacity loss due to film formation. We show that film growth at the negative electrode is faster for charged batteries than for uncharged batteries and that higher electron mobility in the film leads to faster growth. If electron mobility is low, the rate of film growth is limited by transport of electrons through the film, and the rate decreases as the thickness increases. We examine the dependence of film resistance upon both film thickness and defect concentration in the film. We also show that the concentration polarization in the film increases as it grows at open circuit, even though the concentration gradient may decrease.
 [DOI: 10.1149/1.1804812]

Manuscript submitted December 19, 2003; revised manuscript received April 6, 2004. Available electronically October 27, 2004.

Lithium batteries are used as high-energy-density primary and secondary (rechargeable) sources for applications such as cell phones, cameras, and laptop computers. Rechargeable lithium batteries are presently among the leading candidates for hybrid- and electric-vehicle power sources due to their high theoretical capacity, potentially low cost, environmental suitability, and relatively long life.[1]

Lithium batteries come in two varieties, lithium-ion batteries and lithium metal batteries. The former consists of two porous composite electrodes on either side of a porous separator, with current collectors contacting each electrode, as shown in Fig. 1. The composite electrodes consist of polymeric binder, active insertion materials (*e.g.*, graphite in the negative electrode and Mn_2O_4 in the positive electrode), and an electrolytic solution that fills the pores. The solution, which contains a soluble lithium salt, also fills the pores of the separator, thus establishing an electronically insulating, but ionically conducting, contact between the two electrodes. Lithium ions can be inserted into and deinserted from the active insertion materials, and they move from one electrode to the other, depending upon whether the battery is being charged or discharged. The lithium metal battery is analogous to the lithium-ion battery except that the negative (graphitic) electrode is replaced by a thin sheet of lithium metal, which dissolves or deposits lithium depending upon the direction of current flow.

These batteries share another common feature, which contributes to their stability. The so-called solid electrolyte interphase (SEI) layer is a passivating film that forms at the surface of the active electrode material in the battery, protecting the electrolytic solution and other battery components from undesirable reduction or oxidation. (Aurbach gives a fairly comprehensive review of the literature pertaining to the SEI in lithium-ion batteries.[2]) These reactions may involve consumption of active lithium ions, consumption of the solvent, exfoliation of the active electrode material, or gas evolution, which builds pressure in the cell and poses a safety hazard. All of these deleterious effects are considered failure modes of lithium batteries, as they reduce the effective life of the battery.

The composition, structure, and thickness of the SEI layer are strong functions of both the electrode material and the electrolyte (*i.e.*, solution and salt) chemistry.[2,3] In some cases, solvent reduction products lack the characteristics required for effective electrode passivation, and these batteries are prone to failure.[2,3] It is the intent of this work to understand better the role of the SEI layer in battery stability in order to prolong battery life and avoid failure. A mathematical model is presented that can be used to simulate various attributes of the electrode-SEI-electrolyte system in a lithium-ion cell.

Passivating films are common in many electrochemical systems,[2-9] and the first model of the SEI associated with lithium metal electrodes was developed by Bennion and Littauer in 1976.[4] Peled[5,6] further described the passivating film as an ionically conductive, electronically insulating layer at least 1.5 to 2.5 nm thick, the minimal thickness being determined by the electron tunneling range. The film is formed when the electrode first contacts an oxidant, such as air or the solvent of interest.[10] Lithium ions are transported through the film as vacancies or interstitials, while solvent molecules are prevented from reaching the electrode and reacting further. Since the film is, at least to some degree, electronically insulating, continuous solvent reduction at the film-solution interface is prevented. Peled[5,6] derived a parabolic growth law for the SEI based on the assumption that transport of electrons through the SEI is the rate-determining process in SEI growth, although experimentally, films on lithium electrodes do not strictly adhere to the parabolic growth law.

It is presently believed that the SEI on the negative electrode material of Li-metal and Li-ion cells is composed of two distinct layers, a compact polycrystalline or heteromicrophase layer of inorganic products (*e.g.*, Li_2CO_3, LiF, Li_2O, LiCl) that adjoins the electrode material, and a porous, amorphous outer layer composed of partially reduced organic products (*e.g.*, $(CH_2OCO_2Li)_2$, ROLi, $ROCO_2Li$),[11,12] where R is an organic group that depends on the solvent (Fig. 2). The inner (polycrystalline) layer is at least 1.5 to 2 nm in thickness,[5,13] while the outer layer can be on the order of 100 nm thick.[13,14] The exact composition, structure, and thickness depend heavily upon the solution chemistry.[2,3] There is evidence that SEIs form on positive electrode materials (*e.g.*, $Li_yMn_2O_4$, Li_yCoO_2) as well,[2,15] although the focus of the present work is the SEI on the negative electrode, particularly graphite.

Peled has refined his SEI model to include explicitly the presence of grain boundaries between the crystalline particles that make up the inner layer.[16] These grain boundaries impart an added resistance to Li transport perpendicular to current flow,[16] while they may allow swifter transport of lithium ions parallel to current flow.[6] The grain boundaries may also allow transport of some solvent molecules and/or electrons, decreasing the stabilizing effect of the SEI.

The emphasis of the present work is a mathematical description of the SEI on graphitic negative electrodes in lithium-ion batteries. Although the characteristics of passivating films, including chemical composition, are similar for metallic lithium and graphite in contact with identical solutions,[2] there are certain distinguishing features that should be emphasized. For one, the Li-metal electrode undergoes significant volume change as the lithium dissolves into and is deposited from the solution.[17,18] Moreover, lithium can deposit

* Electrochemical Society Student Member.
** Electrochemical Society Fellow.
z E-mail: jake@newman.cchem.berkely.edu

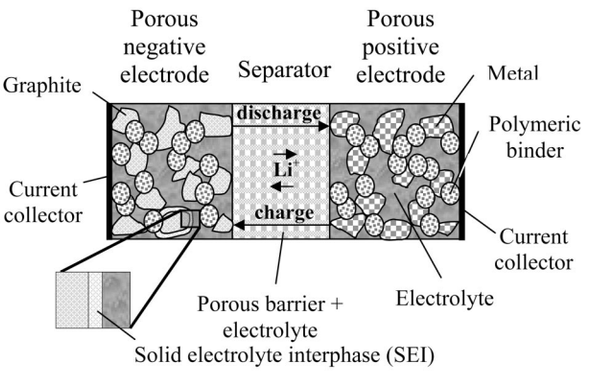

Figure 1. The lithium-ion battery, with two porous electrodes. The SEI layer on graphite is shown in the inset.

within the pores or grain boundaries of the SEI, depending upon its structure,[5,6] or even at the film-solution interface, resulting in fresh film formation at the surface.[6] Prolonged lithium dissolution can also lead to the breakdown and repair of the SEI, which greatly complicates its features, and may result in battery failure (*e.g.*, if dendrites are formed).[2,5]

Graphite, on the other hand, undergoes a much smaller volume change as lithium is inserted into and deinserted from the host graphite, allowing for the presence of a more stable film.[17,18] Whereas the film may be continuously damaged and repaired on lithium-metal electrodes during battery charge-discharge cycling, stable films on graphite generally form during the first one or two cycles,[14,17,19] changing structure only under abusive conditions or during prolonged storage.[20] Initial stability depends, of course, upon the proper selection of carbon type and electrolyte. Finally, while reduction of solution species on lithium metal is somewhat nonselective, resulting in a diverse mosaic of different surface species, surface films are selectively and gradually formed on carbon electrodes as the electrodes are polarized to low potentials.[2,21] This is due to the fact that the vacant graphite starts at a potential of around 2 V *vs.* Li/Li+, and this potential gradually decreases, approaching the potential of lithium metal, as lithium is inserted into the host.

Proposed mechanisms for SEI formation and for battery failure related to unstable SEIs abound in the literature,[3,14,20,22,23] and most of these are somewhat contentious due to the inherent experimental difficulty in characterizing the SEI and lack of fundamental understanding about the nature of SEI formation and evolution. Kinoshita indicates that much of the disagreement stems from the fact that a wide variety of systems is studied under a myriad of conditions, and each combination results in a somewhat unique SEI.[24] The need for a broad, fundamental understanding of the SEI is clear, and a working mathematical model of the SEI should provide a partial means to that end.

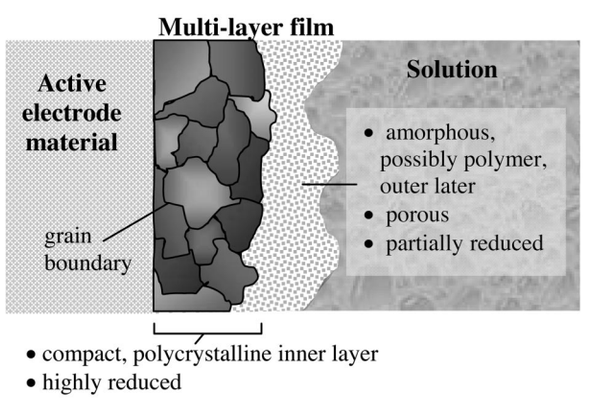

Figure 2. Schematic of the SEI layer on graphite.

The specific objectives of the modeling effort described here include the identification of critical parameters in SEI formation, self-discharge of the negative electrode, film impedance rise, and comparison of simulations with irreversible capacity loss and film impedance data. It is hoped that, in the course of meeting these objectives, the role of the SEI layer in lithium-ion battery operation will become more transparent, and that an improved understanding will help to guide experimental work in the field.

Mathematical Description of the SEI

Most existing models for the SEI on lithium-metal and graphitic electrode materials[4,6,16,21,25-32] neglect variations in film properties and detailed mechanisms for ionic and electronic transport. Many are susceptible to the risks of data fitting, as with the use of RC circuit models to fit ac impedance measurements.[3,16,21,28-32] Heretofore, a continuum mathematical model of the SEI as a mixed conductor has not been developed, although similar models of passivating oxide layers in other electrochemical systems have been constructed.[8,9,33-40]

These models have proposed various rate-limiting processes for oxide film growth, including ionic transport through the film,[34,35] reaction at the film-solution interface,[9,36,37] and reaction at the metal-film interface.[38] Ionic transport in these models has been described by Schottky-defect (vacancy)[35,36,39,40] and Frenkel-defect (interstitial)[39,40] mechanisms of cation[34,35,38-40] and anion[36,39,40] transport. Battaglia and Newman[8] have attempted to combine the relevant mechanisms for growth in a more general oxide growth model that includes transport of cationic and anionic vacancies and interstitials, as well as electrons and holes, through the film.

Gao and Macdonald[39] present an analytic solution based on these principles that explains the impedance behavior of a lithium-polymer cell. While their model explains the phenomenon they observe quite well, it may not describe transient phenomena inherent in film growth, and it is not directly applicable to graphitic electrodes.

The present model draws from those mentioned above, most closely that of Battaglia and Newman, with explicit emphasis on lithium-ion systems with graphitic negative electrodes. The equations employed are similar to those of Battaglia and Newman, with the following distinctions: (*i*) the treatment is simplified with the use of dilute solution theory[7] to compute fluxes in the film, as there is evidence that the film defect concentration is low;[41] (*ii*) an adsorption layer at the inner Helmholtz plane (IHP) of the solution is included in the kinetic scheme; (*iii*) nonequilibrium interfacial kinetic expressions are used in the film boundary conditions; and (*iv*) diffusion of Li in the graphitic host material and variation of potential with state of charge are taken into account.

A further distinction is that Jacobian elements in the present work are derived from governing equations, rather than calculated numerically, which reduces the required computation time considerably.

Governing equations.—Although graphite electrodes are composite electrodes consisting of active graphite particles, a polymeric binder, and electrolyte filling the pores, here we model a one-dimensional film growing on a planar electrode surface (Fig. 3). This can be viewed as an approximation of the surface of an actual graphite particle and a first step toward modeling a porous electrode (see Fig. 1).

In one dimension, the material balance for species k in the film takes the form

$$\frac{\partial c_k}{\partial t} = -\frac{\partial N_k}{\partial x} - \sum_1 s_{k,1} R_1 \qquad [1]$$

where c_k is the concentration of species k, N_k is the molar flux of

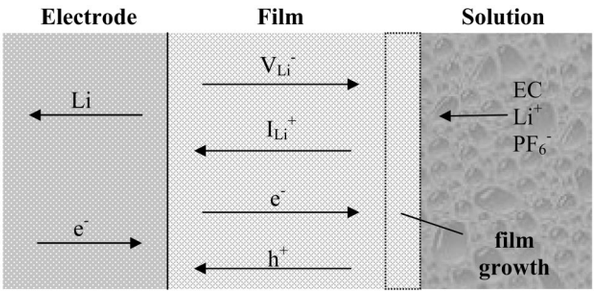

Figure 3. Model of the growing SEI film. V_{Li}^- indicates lithium vacancies, Li_i^+ indicates lithium interstitials, and h^+ indicates holes. Arrows indicate the direction of species motion on charge.

species k, R_1 is the rate of a homogeneous reaction in the film, and $s_{k,1}$ is the stoichiometric coefficient for species k in reaction ℓ.

Given that defects in the film lattice are rare,[41] we employ dilute solution theory[7] to describe the flux of charged species. Accordingly, ions and electrons can move through diffusion, migration, and convection, as described by the flux equation

$$N_k = -D_k\frac{\partial c_k}{\partial x} - z_k\frac{F}{RT}D_k c_k\frac{\partial \Phi}{\partial x} + c_k v_L \qquad [2]$$

We assume that some of the homogeneous film reactions are in equilibrium, for which we use the equilibrium expression

$$K_1 = \prod_k c_k^{-s_{k,1}} \qquad [3]$$

This equation replaces one of the material-balance equations. Thus, the material balances of the species involved in the equilibrium reaction must be combined so that the reaction rate is eliminated from the sum of homogeneous reactions. The combined material balances take the form

$$\sum_k \mu_{i,k}\left(\frac{\partial c_k}{\partial t} + \frac{\partial N_k}{\partial x}\right) = -\sum_1 \nu_{i,1}R_1 \qquad [4]$$

where $\mu_{i,k}$ is a coefficient used to add the material balances such that $\nu_{i,1} = 0$ for each homogeneous reaction ℓ that is in equilibrium. From Eq. 1 and 4, $\mu_{i,k}$ and $\nu_{i,1}$ must satisfy the equation

$$\nu_{i,1} = \sum_k \mu_{i,k}s_{k,1} \qquad [5]$$

For example, if material balance l is that for species l, material balance 2 is that for species 2, material balance 3 is that for species 3, and R_n is the rate of the equilibrium reaction $1 + 2 \rightleftharpoons 3$, then material balance 1 would be replaced by the equilibrium expression $K_n = c_1/(c_2c_3)$, and material balances 2 and 3 could be replaced by combined material balances, where $\mu_{2,1} = 1$, $\mu_{2,2} = -1$, $\mu_{3,1} = 1$, and $\mu_{3,3} = 1$ (the remaining μ's are zero). Thus, from Eq. 5, we have $\nu_{2,n} = 0$ and $\nu_{3,n} = 0$, as desired, and the equilibrium reaction rate is eliminated from both combined material balances. Note that the choices for $\mu_{i,k}$ are not necessarily unique. One might observe that the rate of an equilibrium reaction is zero by definition, so it would seem unnecessary to eliminate such rates from the combined material balances. However, it is necessary to follow this procedure in order to formulate independent equations without any loss of the original material balance constraints.

The above equations are also used to describe transport of solution species. Transport of lithium in the graphite host is limited to solid diffusion

$$\frac{\partial c_{Li}}{\partial t} = \frac{\partial}{\partial x}\left(D_S\frac{\partial c_{Li}}{\partial x}\right) \qquad [6]$$

The potential in the film and solution can be treated in one of two ways. The electroneutrality approximation

$$\sum_k z_k c_k = 0 \qquad [7]$$

does fairly well when the diffuse space-charge region (characterized by the Debye length) is small.[7] However, for a Li_2CO_3 film with 10^{-3} M lithium-ion interstitials and electrons, the Debye length is

$$\lambda = \sqrt{\frac{\varepsilon RT}{F^2\Sigma_k z_k^2 c_k}} = 2.4 \text{ nm} \qquad [8]$$

which represents a significant fraction of a film that is tens of nanometers thick. Here, ε is the electric permittivity of the film, R is the ideal-gas constant, and F is Faraday's constant. In this case, it may be appropriate to use the more rigorous Poisson's equation in place of electroneutrality

$$\frac{d}{dx}\left(\varepsilon\frac{d\Phi}{dx}\right) = -F\sum_k z_k c_k \qquad [9]$$

Replacing Eq. 7 with Eq. 9 requires the addition of boundary conditions on either side of the film, and it increases the nonlinearity and complexity of the set of equations to be solved. Due to difficulties in achieving convergence, Eq. 7 is used for the simulations presented in this paper, although convergence with Eq. 9 has been achieved in some cases. The effect of the space-charge region in the film is mitigated at lower electrode potentials (higher states of charge), since the films grow faster (see Fig. 9) and the concentration of charged species in the film is higher.

Since the conductivity of electrons in the graphite is constant, Laplace's equation is obeyed for the potential there

$$\frac{d^2\Phi}{dx^2} = 0 \qquad [10]$$

Finally, the film lattice velocity is defined by the flux of lattice sites (vacancies and occupied sites) divided by the concentration of lattice sites

$$v_L = \frac{\Sigma_k^{\text{Li sites}} N_k}{\Sigma_k^{\text{Li sites}} c_k} \qquad [11]$$

Lattice sites include filled sites and vacancies, but not interstitials. This is basically a continuity equation for the lattice, as a summation of Eq. 1 for all species occupying a particular type of lattice site (*e.g.*, lithium), or all lattice sites, and substitution into Eq. 11, yields

$$\frac{\partial}{\partial t}\left(\sum_k^{\text{Li sites}} c_k\right) + \frac{\partial}{\partial x}\left(v_L\sum_k^{\text{Li sites}} c_k\right) = 0 \qquad [12]$$

The homogeneous reaction rates cancel because lattice sites can only be generated or destroyed at the film boundaries. Equation 12 allows for films of varying site density; however, in the absence of data pertaining to density variation, we shall assume that the density is constant.

Coordinate transformation.—In order to account for a variable film thickness, the following coordinate transformation is employed. We first define a dimensionless distance from the electrode/film interface

$$\xi = \frac{x}{L} \qquad [13]$$

where L is the thickness of the film and is a function of time. Spatial derivatives simply become

$$\left(\frac{\partial c}{\partial x}\right)_t = L(t)\left(\frac{\partial c}{\partial \xi}\right)_t \quad [14]$$

while time derivatives take the form

$$\left(\frac{\partial c}{\partial t}\right)_x = \left(\frac{\partial c}{\partial \xi}\right)_t \left(\frac{\partial \xi}{\partial t}\right)_x + \left(\frac{\partial c}{\partial t}\right)_\xi \left(\frac{\partial t}{\partial t}\right)_x = \frac{\partial c}{\partial t} - \frac{\xi}{L(t)}\frac{\partial L}{\partial t}\frac{\partial c}{\partial \xi} \quad [15]$$

Our material balance for species k becomes

$$\frac{\partial c_k}{\partial t} - \frac{\xi}{L(t)}\frac{\partial L}{\partial t}\frac{\partial c_k}{\partial \xi} + \frac{1}{L(t)}\frac{\partial N_k}{\partial \xi} + \sum_1 s_{k,1}R_1 = 0 \quad [16]$$

If the film growth rate dL/dt is slow, the second term can be neglected, and Eq. 1 is recovered, so long as the distance between nodes used in the finite difference scheme is recalculated at each timestep. This is a form of a pseudo-steady-state calculation.

Boundary conditions.—At the boundaries, the material balances take the form

$$\pm(N_k - c_k v_I) = -\sum_1 s_{k,1}R_{Al} \quad [17]$$

where R_{Al} is the rate of heterogeneous reaction ℓ and $s_{k,1}$ is the stoichiometric coefficient of species k in reaction ℓ (see Eq. 23, below). v_I is the interfacial velocity, which is related to the lattice velocity by

$$v_I = v_L \pm \frac{\Sigma_k^{\text{all sites}}\Sigma_1 s_{k,1}R_{Al}}{\Sigma_k^{\text{all sites}}c_k} \quad [18]$$

In Eq. 17 and 18, the positive sign corresponds to the right side of an interface (*e.g.*, the electrode-film interface), and the negative sign corresponds to the left. The last term on the right side of Eq. 18, rewritten as

$$\frac{\Sigma_1 R_{Al}\Sigma_k^{\text{all sites}}s_{k,1}}{\Sigma_k^{\text{all sites}}c_k} \quad [19]$$

indicates that film growth proceeds only with reactions for which the sum of stoichiometric coefficients of lattice species is nonzero.[33]

For species adsorbed at the IHP of the solution, the material balance is

$$\frac{d\Gamma_k}{dt} = -\sum_1 s_{k,1}R_{Al} \quad [20]$$

where Γ_k is the surface concentration of species k, in moles per unit area.

As alluded to earlier, the use of Poisson's equation would require additional boundary conditions for the potential, namely, Gauss' law. In one dimension, Gauss's law takes the form

$$\varepsilon\left.\frac{d\Phi}{dx}\right|_{\text{left}} - \varepsilon\left.\frac{d\Phi}{dx}\right|_{\text{right}} = F\sum_k z_k\Gamma_k \quad [21]$$

which illustrates that the difference in electric field on either side of a plane is proportional to the charge on the plane. If δ_1 is the distance from the film's outer Helmholtz plane (OHP) to the solution's IHP and δ_2 is the distance from the solution's IHP to the solution's OHP, Eq. 21 for the left side of the film/IHP interface can be approximated as

$$\varepsilon_{\text{film}}\frac{\Phi_{\text{IHP,sol}} - \Phi_{\text{OHP,film}}}{\delta_1} - \varepsilon_{\text{sol}}\frac{\Phi_{\text{OHP,sol}} - \Phi_{\text{IHP,sol}}}{\delta_2} = F\sum_k z_k\Gamma_k \quad [22]$$

Similar equations can be written for each side of each interface. When electroneutrality (Eq. 7) is used in place of Poisson's equation, these boundary conditions are not required.

The potential or current must be set at one end of the system. Since the zero of potential is arbitrary (only differences in potential can be measured), it is convenient to set the potential to zero on the right side of the solution phase, where a reference lithium electrode is located. For galvanostatic or potentiostatic simulations, the current or potential, respectively, can be set at the left side of the graphite particle.

The solution phase to the right of the film is assumed to be stagnant near the film, but well-mixed far from the film, so that the species concentrations at the far right are approximately constant. These bulk concentrations are specified parameters of the model. The velocity of the solution normal to the film is equal to the velocity of the film/solution interface, or v_I.

Special boundary conditions must also be set for the initial ($t = 0$) solution. Since the initial film species concentrations cannot be determined from the flux boundary conditions at each interface, their average concentrations, or the concentrations at one end of the film, must be specified. For the simulations described here, the initial film concentrations and surface concentrations of adsorbed species are specified.

Kinetics.—Following the formalism of Newman,[7] a general charge-transfer surface reaction can be written as

$$\sum_k s_k M_k^{z_k} \rightarrow 0 \quad [23]$$

where s_k is the stoichiometric coefficient for species k ($s_k > 0$ for anodic reactants) and z_k is the charge number of that species. Note that no explicit mention of electrons has been made, since they are treated here as reacting species. The amount of charge transferred is then

$$n = -\sum_k^{\alpha} s_k z_k = \sum_k^{\gamma} s_k z_k \quad [24]$$

where α designates the phase to the left of the interface and γ the phase to the right.

Butler-Volmer expressions[7] are used to describe all charge-transfer reactions

$$R_{Al} = \frac{i_1}{n_1 F} = k_{a,1}\prod_k^{\text{reactants}} c_k^{s_{k,1}} \exp\left[(1-\beta_1)\frac{n_1 FV}{RT}\right] - k_{c,1}\prod_k^{\text{products}} c_k^{-s_{k,1}} \exp\left[-\beta_1\frac{n_1 FV}{RT}\right] \quad [25]$$

where k_a and k_c are forward (anodic) and reverse (cathodic) rate constants, respectively, β is a symmetry factor, and V is the potential just to the left of the interface minus the potential just to the right.

Note that Eq. 23 to 25 apply equally well to surface reactions that do not involve charge transfer. In that case, $n = 0$, and there is no potential dependence in Eq. 25.

Reaction mechanism.—To keep the reaction scheme simple, we adopt a portion of the mechanism proposed by Aurbach[3] for the formation of a Li_2CO_3 film on graphite with an electrolytic solution of 1 M $LiPF_6$ in a mixture of ethylene carbonate (EC) and dimethyl carbonate (DMC). Although the complete mechanism includes formation of $(CH_2OCO_2Li)_2$ via disproportionation, particularly when the EC content in the solvent is high, we neglect this for the present,

perhaps including its formation in future simulations. The following are the elementary steps in film formation, where S represents a surface site.

Adsorption reactions.—

$$EC(sol) + S \rightleftharpoons EC(ads) \quad [26]$$

$$Li^+(ads) \rightleftharpoons Li^+(sol) + S \quad [27]$$

$$C_2H_4(gas) + 2S \rightleftharpoons C_2H_4(ads) \quad [28]$$

Charge-transfer reactions at the solution IHP.—

$$EC^-(ads) \rightleftharpoons EC(ads) + e^-(film) \quad [29]$$

$$C_2H_4(ads) + CO_3^{2-}(ads) \rightleftharpoons EC^-(ads) + e^-(film) + 2S \quad [30]$$

Film formation.—

$$CO_3^{2-}(ads) + 2Li^+(ads) \rightleftharpoons Li_2CO_3(film) + 3S \quad [31]$$

In addition to film formation, the model must also include surface reactions that facilitate transport of ionic and electronic species through the film. On the solution side of the film, these include

$$Li_{Li} + S \rightleftharpoons V_{Li}^- + Li^+(ads) \quad [32]$$

$$Li_i^+ + S \rightleftharpoons Li^+(ads). \quad [33]$$

Kroger-Vink notation is used to represent the film species.[9,35,39] V_{Li}^- refers to lithium vacancies, Li_i^+ to lithium interstitials, and Li_{Li} to lithium-filled lithium sites. Since transport of CO_3^{2-} as either vacancies or interstitials is unlikely,[41] the associated surface reactions are omitted.

At the graphite/film interface, lithium is inserted into and deinserted from the graphite host from and to the film lattice. Furthermore, electrons can be transferred from the electrode material to the film. Thus, the following three reactions occur at the graphite/film interface

$$e^-(film) \rightleftharpoons e^-(electron) \quad [34]$$

$$LiC_6 + V_{Li}^- \rightleftharpoons Li_{Li} + e^-(electron) + C_6 \quad [35]$$

$$LiC_6 \rightleftharpoons Li_i^+ + e^-(electron) + C_6 \quad [36]$$

Notice that, in Reaction 34, the forward rate in Eq. 25 depends upon the concentration of electrons in the film, while the reverse rate does not depend on any concentration, the activity of electrons in the graphite being set to unity. Likewise, the rates of Reactions 35 and 36 are independent of electron concentration. Furthermore, the reverse rates of these reactions depend on the concentration of vacant graphite host sites, or $c_{Li,max} - c_{Li}$, where $c_{Li,max}$ is the maximum allowable concentration of lithium in the graphite host, corresponding to a state of charge (SOC) equal to one, or one lithium atom for every six carbon atoms. $x_{Li} = c_{Li}/c_{Li,max}$ is the SOS of the graphite, or fraction of intercalation sites that are filled.

Parameters of the model.—Properties of the film were chosen to be those of Li_2CO_3. Although it remains in question whether this is a major constituent of a real SEI in a lithium ion battery,[2] it is the favored thermodynamic product,[12] and may be present close to the graphite even if it is not detectable. Lattice parameters from the literature[41] were used to estimate the film density and concentration of sites, as well as the concentration of adsorption sites at the film/solution interface. The equilibrium constant for lithium vacancy-interstitial generation was also estimated from the literature.[41] The bulk lithium interstitial concentration and diffusion coefficient were estimated from another source.[27] The bulk vacancy concentration can be calculated from the interstitial concentration and the equilibrium constant.[41] The result that the interstitial concentration is several orders of magnitude greater than the vacancy concentration is in good agreement with the conclusion that interstitials are the majority carrier,[41] even should the two have comparable mobilities. It was assumed that the vacancy diffusion coefficient is equal to the interstitial diffusion coefficient. For solid ionic conductors, vacancy diffusivities are typically several orders of magnitude lower than interstitial diffusivities. However, in our simulations vacancy transport is already insignificant due to the much higher concentration of interstitials, and thus lowering the vacancy diffusivity would have a negligible impact on the results.

As discussed below, another set of equilibrium concentrations is consistent with both the vacancy/interstitial equilibrium constant and the finding that interstitials are the majority carrier. Since the bandgaps of inorganic lithium compounds (*e.g.*, LiF and LiCl) are generally quite large, we expect a very low concentration of electrons (and holes) in the film. Thus, electroneutrality would dictate that the concentration of vacancies be equal to the concentration of interstitials, set by the equilibrium relationship. In order to maintain a high transference number of interstitials, the diffusion coefficient of vacancies could be made much lower than that of interstitials. Although the present results do not reflect this choice in parameters, future results will.

The electrolytic solution is assumed to be 1 M $LiPF_6$ in an idealized solution of reacting EC and inert DMC. To simplify the model, the PF_6^- anion is also considered an inert species, despite evidence that $LiPF_6$ dissociates into LiF and PF_5, a strong Lewis acid.[22] The diffusion coefficients for Li^+ and PF_6^- in the mixture are set at 5×10^{-6} cm^2/s,[42] assuming that Li^+ and PF_6^- have the same diffusivity.

The solid-state lithium diffusion coefficient and electrical conductivity of graphite are borrowed from previous battery simulations involving a graphite negative electrode.[43] Following Ref. 43, the electrical conductivity of the graphite is set arbitrarily high, to a value of 0.1 S/cm, for the simulations described here. It remains to estimate, guess, or fit the values of the various interfacial kinetic parameters. Measurement of these parameters is hindered by the slow diffusion of lithium in the graphite coupled with fast charge-transfer processes.[43] In the absence of experimental data, all values of β in the Butler-Volmer expressions are taken to be 1/2; that is, we assume the applied potential drives anodic and cathodic processes equally.[7] The two rate constants for each reaction can be written in terms of a single rate constant (k_a) and an equilibrium constant (K)

$$k_{c,1} = K_1 k_{a,1} \quad [37]$$

It therefore seems to be a superior strategy to set the equilibrium constant for each reaction, then vary the single rate constant parametrically, rather than haphazardly vary both rate constants. In fact, physical intuition may allow us to estimate some of the equilibrium constants with some degree of accuracy. For instance, the equilibrium constants for Reactions 27, 33, and 36 are related to the overall lithium intercalation equilibrium constant by

$$K_{global} = K_{27} K_{33} K_{36} \quad [38]$$

under conditions in which the concentration of interstitials is uniform throughout the film. Similarly

$$K_{global} = K_{27} K_{32} K_{35} \quad [39]$$

The overall equilibrium constant has been estimated from a fit of the open-circuit potential (OCP) as a function of SOC, as provided by Bellcore (now Telcordia) for graphite.[44]

The above equilibrium constants are further constrained by the requirement that the concentrations of lithium vacancies and interstitials must be in equilibrium at either end of the film, as well as throughout the film

$$K_{eq} = c_{V_{Li}^-} c_{Li_i^+} = K_{33}/K_{32} = K_{35}/K_{36} \quad [40]$$

Table I. Physical parameters used in the model.

Parameter	Graphite	Ref.	Film (Li_2CO_3)	Ref.	Solution (1 M $LiPF_6$ in EC)	Ref.
D (cm^2/s)	5×10^{-9} (for coke)	45	10^{-10} to 10^{-9} Li_i^+	27	5×10^{-6}	42
σ (S/cm)	0.1	[a]	—	—	—	—
ρ (g/cm^3)	1.8	43	2.11	46	1.34	47
$\varepsilon/\varepsilon_0$	—	—	4.9	28	89.6	47
K_{eq} for V_{Li}^-/Li_i^+ generation (mol^2/m^6)	—	—	7.48×10^{-6}	41	—	—

[a] The electrical conductivity is assigned an arbitrarily high value, as in Ref. 43.

Three of the four equilibrium relations listed above are independent of each other. Thus, two of the five equilibrium constants, K_{27}, K_{32}, K_{33}, K_{35}, and K_{36}, can be specified independently, with the exception of the pairs (K_{32},K_{33}) and (K_{35},K_{36}).

Alternatively, one could assure thermodynamic consistency by specifying secondary reference states for each of the species involved in the set of reactions. One would then calculate equilibrium constants from the secondary reference states, as outlined in Chapter 23 of Ref. 7.

A summary of model parameters, estimated or derived from the literature, is given in Tables I and II.

Results and Discussion

Figure 4 illustrates the growth characteristics at open circuit (zero current) for films with different electronic transference numbers. The transference number of a charge-carrying species is defined as the fraction of current carried by that species in the absence of concentration gradients, and is given by the equation[7]

$$t_k^0 = \frac{z_k^2 D_k c_k}{\Sigma_i z_i^2 D_i c_i} \qquad [41]$$

where the superscript 0 refers to the species, in this case the occupied lattice site, whose velocity is used as a reference velocity. It is clear from Fig. 4 that the rate of film growth increases with electronic transference number, but only to a point.

The fact that film growth depends on the electronic transference number only below a critical value implies that other mechanisms, such as the interfacial kinetics, are rate-limiting when it is above that value. This is confirmed by the slopes of the film-growth curves in Fig. 4. The curves for $t_e^0 = 0.1$, 0.2, and 0.4 are linear, while it is evident that the curve for $t_e^0 = 10^{-4}$ starts to bend over. (The curves for $t_e^0 = 10^{-3}$ and 10^{-5} also bend over slightly, although this is difficult to see in the figure.)

Peled[5,6] hypothesizes that it is transport through the passivating film that limits its growth on the electrode. Accordingly, it is expected that the film adheres to a parabolic growth law.[2,5,6] Although the curve for $t_e^0 = 10^{-4}$ does not fit the parabolic equation given in Ref. 6, the fact that it bends over is equivalent to the increased importance of a transport limitation. The diffusion resistance for all species becomes greater as the film thickness increases. A higher electronic diffusion resistance, when it is rate-limiting, means slower growth.

Figure 5 is a schematic of the electron concentration through the film after the concentration profile is well established. There are three major film-growth limitations depicted in the drawing, a kinetic limitation at the electrode/film interface, a mass-transport limitation within the bulk of the film, and another kinetic limitation at the film/solution interface. (The detail of the solution IHP in the film-growth mechanism has been omitted in order to simplify the argument.) At each interface, an equilibrium concentration of electrons can be derived from the detailed kinetic mechanism and Eq. 25. The equilibrium concentrations depend only on the concentrations of relevant species in the electrode and solution, which, for the sake of argument, we assume are constant. The rate of electron transfer across each interface is proportional to the difference between the film surface concentration and equilibrium concentration of electrons. The film growth rate, in turn, is proportional to the rate of electron transfer. In the absence of mass-transfer limitations, the

Table II. Assumed kinetic and thermodynamic parameters. Equilibrium constants for reactions 27, 32, 33, 35, and 36 satisfy Eq. 23 to 25. The values of K_{35} and K_{36} given here correspond to an SOC of 0.99 (see Fig. 7 and 8), but they are SOC-dependent and are calculated from the OCP function and Eq. 38 and 39.

Reaction	β	$K = k_c/k_a$	k_a
26	—	9×10^6 mol/m^3	10^8 $m^3/mol\text{-}s$
27	0.5	10^{-5} m^3/mol	10^{13} s^{-1}
28	—	1 mol^2/m^5	10^8 $m^2/Pa\text{-}mol\text{-}s$
29	0.5	1 m^3/mol	10^{11} s^{-1}
30	0.5	1 m^5/mol^2	10^8 $m^2/mol\text{-}s$
31	—	10^{-45}	10^{28} $m^4/mol^2\text{-}s$
32	0.5	1.34×10^5 m^3/mol	7.48×10^{-6} s^{-1}
33	0.5	1 mol/m^3	1 $m^3/mol\text{-}s$
34	0.5	10^7 mol/m^3	10^{-12} m/s
35	0.5	0.787 mol/m^3	1.02×10^{-13} $m^4/mol\text{-}s$
36	0.5	1.05×10^5 m^3/mol	1.02 m/s

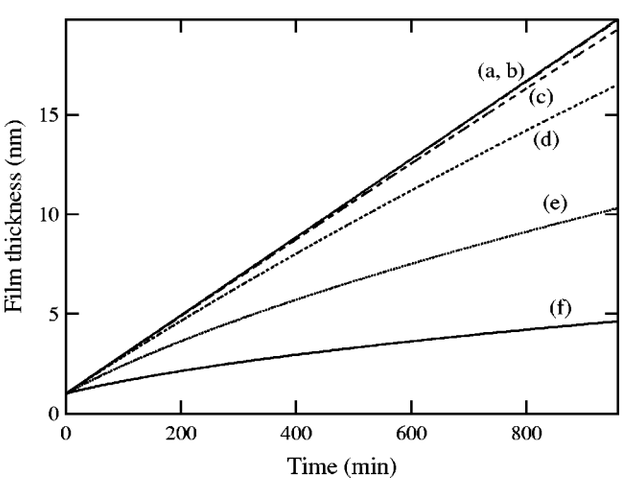

Figure 4. Film growth at open circuit (initial SOC = 0.2). The electronic transference number was set to (a) 0.4, (b) 0.1, (c) 10^{-2}, (d) 10^{-3}, (e) 10^{-4}, and (f) 10^{-5}.

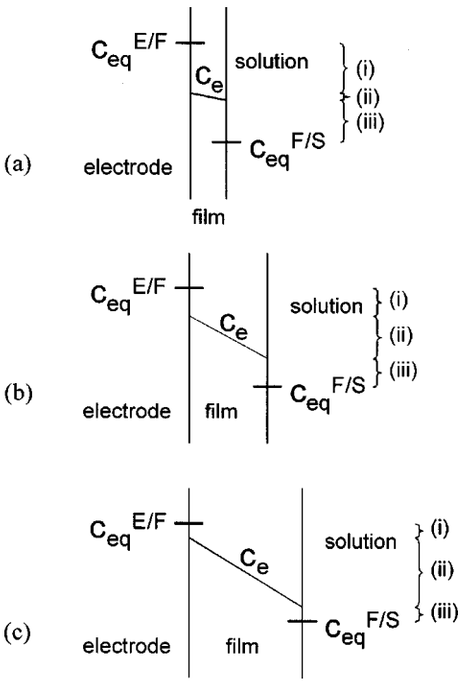

Figure 5. Schematic of kinetic and diffusive transport resistances in a growing film at (a) short time, (b) intermediate time, and (c) long time. $c_{eq}^{E/F}$ is the equilibrium concentration of electrons at the electrode/film interface, and $c_{eq}^{F/S}$ is the equilibrium concentration of electrons at the film/solution interface. The brackets represent concentration differences that correspond to (i) a kinetic resistance at the electrode/film interface, (ii) mass-transfer (diffusion and migration) resistance, and (iii) a kinetic resistance at the film/solution interface.

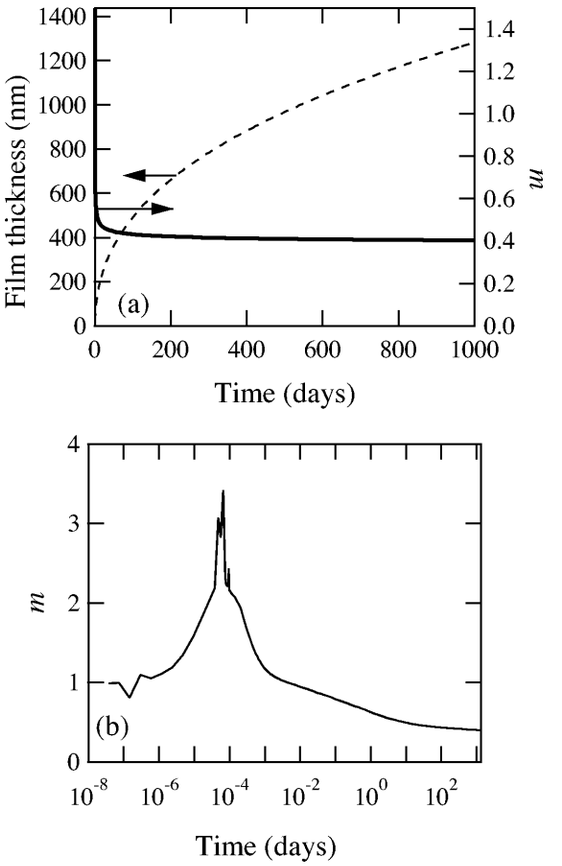

Figure 6. (a) Film growth and evolution of the growth law exponent (m) during open-circuit self discharge (initial SOC = 0.99, $t_e^0 = 10^{-4}$). (b) m plotted *vs.* time on a log scale.

concentration of electrons in the film will remain constant, so the rate of electron transfer will also be constant. Thus, film growth will be in a linear regime.

If there is a mass-transfer limitation in the film, its magnitude will increase as the film grows. Likewise, as the flux of electrons decreases, the concentration of electrons in the film at each interface will approach the equilibrium value, and the kinetic limitations will decrease. Thus, at short times (Fig. 5a), we expect to see kinetically controlled film growth, and at long times (Fig. 5c), film growth will be limited by mass transport. This is true regardless of the mobility of electrons in the film, although the relative time scales depend upon the mobility. At intermediate times (Fig. 5b), film growth may be controlled by the kinetics as well as mass transport. We would then expect film growth behavior to fall somewhere between linear and parabolic. This is precisely what is shown in Fig. 4 when $t_e^0 < 0.2$.

Figure 6 shows film thickness increasing over a period of 1000 days, as well as the order of t in the film-growth equation $L(t) - L_0 = At^m$. The initial film thickness is subtracted from the transient film thickness in order to emphasize that initially there are no mass-transfer limitations, since the concentration of electrons in the film is uniform. It is evident from the figure that film growth is indeed linear ($m = 1$) at short times, and becomes increasingly parabolic ($m = 1/2$) at longer times. However, the value of m approaches a value of 0.4 rather than 0.5 at very long times. This is due to the dramatic decrease in electrode SOC, which decreases the potential and driving force for film growth, over the period of 1000 days.

There is also a period of film growth acceleration ($m > 1$) at very short times ($t < 6$ min) shown in Fig. 6b. This can be explained by the fact that there is a greater difference between the equilibrium electron concentration at the electrode/film interface and the initial electron concentration than there is between the initial electron concentration and the equilibrium concentration at the film/solution interface. Thus, the average concentration in the film increases for a short period before the concentrations at either end approach their equilibrium values, and the rate of reduction of IHP species increases, accelerating film growth, during this period. There is some roughness and oscillation in m at short times due to the discrete nature of the simulation time stepping and the manner in which m was calculated.

Figure 7 shows the concentration profile of lithium interstitials and electrons in the film at various times during film growth. When plotted against the dimensionless distance from the electrode (Fig. 7a), it is clear that the relative concentration polarization increases with time, in agreement with the conclusion that film growth is becoming transport limited. When the concentration profiles are plotted against dimensional distance in the film from the electrode (Fig. 7b), it is evident that the concentration gradient actually decreases with time. However, owing to the increased film thickness, the overall concentration polarization in the film increases as the film grows, although its rate of increase falls off. These are characteristics of the transition from kinetically limited to transport-limited growth.

The rate of film growth at open circuit can also be influenced by the SOC at which the battery is stored, as shown in Fig. 8. As one might expect, at a higher SOC (lower electrode potential), the film grows faster. Figure 9, which shows film thickness and SOC *vs.* OCP, illustrates that the film growth varies smoothly with potential, even though the SOC does not. Thus, the OCP is a better determinant of film growth rate than is the SOC. At lower electrode potentials, the rate of electron injection into the film, and therefore the

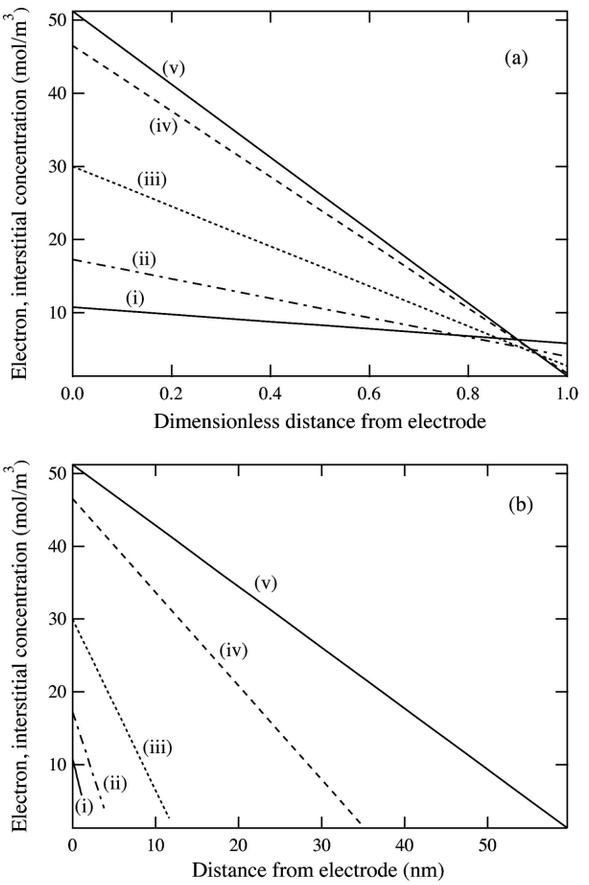

Figure 7. Electron and lithium interstitial concentrations in the film, as a function of (a) dimensionless distance from the electrode and (b) actual distance from the electrode. The concentration profiles correspond to open-circuit film growth (SOC = 0.99, $t_e^0 = 10^{-4}$) after (i) 1 min, (ii) 33 min, (iii) 2.8 h, (iv) 13.9 h, and (v) 29.2 h.

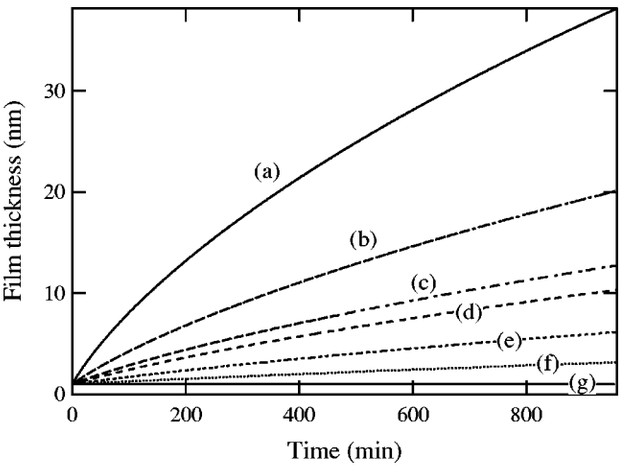

Figure 8. Film growth at open circuit ($t_e^0 = 10^{-4}$). The initial SOC was (a) 0.99, (b) 0.9, (c) 0.8, (d) 0.5, (e) 0.2, (f) 0.1, and (g) 0.01.

driving force for solvent reduction, is higher. This increase in the rate of electron injection can be seen as a consequence of the potential dependence in the Butler-Volmer equation that governs the interfacial kinetics. At open circuit, the cathodic (solvent-reduction) process is balanced by the oxidation of the graphite electrode, which is manifested as self-discharge (deinsertion of lithium).

Figure 10a shows the capacity loss due to film formation and decrease in film resistivity corresponding to the initial SOC = 0.99 curve in Fig. 8, while Fig. 10b compares the rates of film growth and impedance rise. It is apparent that, although the film grows from 1 to 50 nm within 25 h, the capacity in the electrode decreases by only 0.6%. As stated above, this is due to the fact that the overall film thickness is small compared to the size of the model graphite particle. We might expect a greater percentage of capacity loss if the graphite particle were a sphere, 10 μm in diameter, rather than a 10 μm thick planar electrode. In this case, the same film thickness would represent a 3.6% loss, six times that of the planar electrode. If the particle size were reduced to 3 μm, this figure would increase to 12%, which is in better agreement with experimentally measured capacity loss.[30,48-54]

The capacity decline shown in Fig. 10a is due to two separate phenomena. One is evidently growth of the film, as lithium from the electrode is consumed in this process. The other is net injection of interstitial lithium ions into the film, since our simulations show that the concentration of interstitials in the film increases with time. In terms of the argument depicted in Fig. 5, this increase is due to the initial interstitial concentration being closer to the equilibrium concentration at the film/solution interface than that at the electrode/film interface. If the opposite had been the case, the average interstitial concentration would have decreased with time.

Transport of lithium from the electrode to the film in the form of interstitial ions cannot be defined as capacity loss, per se, since the interstitial ions are still available for cycling during charge and discharge. At a higher electrode potential, the average concentration of interstitials in the film would decrease as lithium is inserted into the electrode. In any case, the fraction of lithium removed from the electrode that manifests itself as increased interstitial concentration is negligible (4.4×10^{-2}% after 26 h), since the average concentration of interstitial lithium ions is still very small compared to that of filled lithium sites. The advantage of Li transfer from the electrode to the film is that it increases the conductivity of the film considerably.

Of greater concern is the irreversible capacity loss (*ICL*) associated with Li consumption during film formation. *ICL* can be divided into two general phenomena, loss of cyclable lithium, which shifts the path traced out within the cell's state-of-charge operating window,[55] and loss of active electrode material, via exfoliation, electronic isolation, or other phenomena. Growth of a lithium-containing

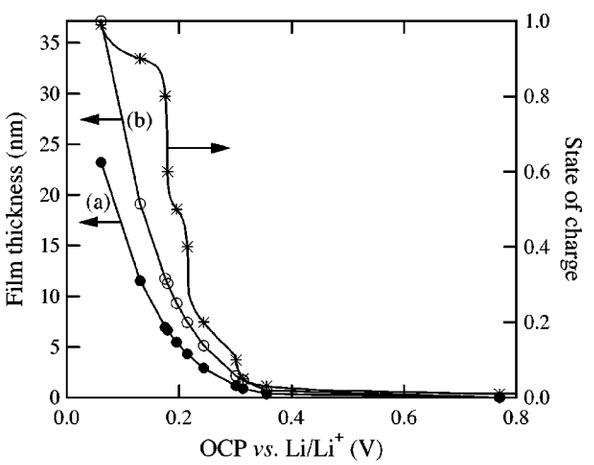

Figure 9. Film thickness (a) after 8 h and (b) after 16 h and graphite state of charge as functions of OCP. The markers indicate potentials at which film growth was simulated. The SOC curve is from an empirical fit.[44]

SEI on the negative electrode is an example of the former type of *ICL*, which can be compensated for by mismatching the electrode capacities during cell assembly.[19,55]

Zaghib *et al.* showed that *ICL* decreased with increasing particle size, due to the increased surface area associated with smaller particles, and that it also depended upon the fraction of edge sites *vs.* basal-plane sites.[56] Shim and Striebel were able to decrease *ICL* for natural and synthetic graphites by pressing the electrodes, which reduced the electrode/solution interfacial area.[48] It would then seem that a larger particle size is advantageous, since irreversible capacity fade diminishes, as a percentage of total initial capacity, as we increase the size of the particle. However, a smaller particle size implies a larger reaction surface between the electrode active material and electrolyte, and transport limitations in both the graphite and solution are minimized. The optimal particle size would depend upon the particular battery application. High-power batteries (*e.g.*, for hybrid-electric vehicles) cannot afford to have additional transport limitations, but could be built with more excess capacity, so a smaller particle size seems ideal. On the other hand, size limitations on high-energy batteries (*e.g.*, for pure electric vehicles) may preclude building in a lot of excess capacity, while slower transport may not be as detrimental, so a larger particle size would be suitable. Existing porous electrode models[43] could be used to examine this trade-off.

Zaghib *et al.* determined that the *ICL* on edge sites in natural graphite was 35 mAh/m^2, and on basal-plane sites was 7 mAh/m^2, in general agreement with other normalized *ICL* figures reported in the literature.[32,49,57,58] A simple charge balance gives the normalized *ICL* in terms of the SEI thickness, assuming all *ICL* is due to film formation, and that the SEI is sufficiently thin compared to the electrode particles that we can approximate it as planar

$$ICL = \frac{nFL\rho}{MW} \qquad [42]$$

n is the number of electrons transferred per film unit (*i.e.*, one molecule of Li_2CO_3) generated, and *MW* is the molecular weight of a single film unit. Assuming the properties of Li_2CO_3, the area-specific *ICL* is equivalent to 1.5 *L*, where *L* is given in nanometers and *ICL* in mAh/m^2. Given the *ICL* figures cited above, we would expect a 23 nm Li_2CO_3 film to form on edge sites of graphite, and a 5 nm film to form on basal-plane sites. These values are within the range of simulated thickness shown in Fig. 4 and 8 and within the range of values reported in the literature.[14,23,27,28,50,51,59,60] Thicker films may correspond to reduction products with lower density, higher molecular weight, or a smaller value of *n* than Li_2CO_3. Polymeric solvent-reduction products may exhibit all three of these properties.

Figure 10b demonstrates that, in the first several hours, the film resistance at open circuit bends over more sharply than does the film thickness. This feature can be explained by the fact that the average conductivity of the film, which increases with the concentration of lithium interstitials, nearly doubles during the interval between 30 s and 2 h. Thus, although lithium ion injection into the film has a negligible effect on overall capacity loss, it can have a dramatic effect on film resistance. A desirable property of the SEI, then, is that it should have the capacity to sustain high concentrations of lithium-ion defects. Solvents and solution additives should be chosen with this in mind.

The average ionic resistivity, $\overline{\rho}_{Li}$, plotted in Fig. 10a, is calculated from the equation

$$\overline{\rho}_{Li} = \overline{1/\kappa_{Li}} = \frac{RT}{F^2 z_{Li}^2 D_{Li}} \overline{1/c_{Li}} \qquad [43]$$

where the overbar signifies a distance-averaged value. When the concentration of a species is uniform, its conductivity is a proportionality constant relating the potential gradient to the current carried by that species[7]

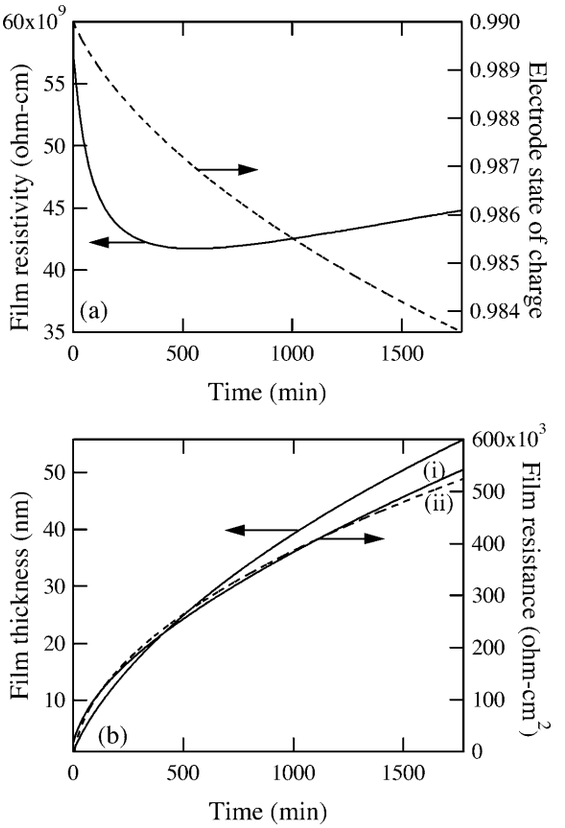

Figure 10. (a) Change in SOC and film resistivity at open circuit ($t_e^0 = 10^{-4}$). (b) Film growth and (i) impedance rise, with (ii) a parabolic fit for the film impedance ($R = 500{,}844t^{1/2} - 31{,}294$).

$$i_k = -\kappa_k \frac{\partial \Phi}{\partial x} \qquad [44]$$

Hence, in the absence of concentration gradients

$$\overline{\rho}_{Li} = \overline{1/\kappa_{Li}} = \left|\frac{\Delta\Phi}{i_{Li}L}\right| = \frac{R_{Li}}{L} \qquad [45]$$

where R_{Li} is the ionic resistance of the film and $\Delta\phi$ is the potential difference across the film. This relationship does not apply when there are concentration gradients, as we have in the present case; the average resistivity shown in Fig. 10a is, therefore, not simply the ratio of ionic resistance to film thickness, both of which are shown in Fig. 10b. An interesting feature of the film resistivity is that it reaches a minimum at 549 min, then gradually increases. This coincides with a gradual decrease in concentration of mobile charge carriers near the film/solution interface, where the high resistivity dominates the average.

The values of the film resistance shown in Fig. 10 are at the high end of the range of SEI resistances reported in the literature.[3,15,16,20,21,27-32,49,61-63] Most authors, if they normalize impedance values at all, report resistances in Ω-cm^2, corresponding to the cross-sectional area of the electrode. In order for comparison with the results shown here, experimentally measured values must be converted to an electrode-surface-area basis by multiplying the reported values by the factor *aL*, where *a* is the electrode-solution interfacial area per electrode volume and *L* is the porous electrode thickness.[7] Often, values of *a* are not reported, but they can be estimated from the equation

$$a = \frac{3\varepsilon_a}{r} \quad [46]$$

where ε_a is the active material volume fraction and r is the particle radius. Here we have assumed a spherical particle morphology. Some of the carbon particles used in these studies were graphite flakes, which do not have a spherical geometry. However, since only a nominal particle size, rather than the particle dimensions, was reported, we have used Eq. 46 in all cases. When the active-material volume fraction was not reported or could not be calculated from other parameters, we assumed a value of 0.4.

Markovsky *et al.*[61] measured an approximately tenfold increase in resistance of an electrode composed of mesocarbon microbeads (38%) and mesocarbon fibers (56%) stored at 25°C and 170 mV *vs.* Li/Li^+ for 610 h. By our estimations, their film resistance grew to 1800 Ω-cm^2 (based on interfacial area) after 27 h, and 10,000 Ω-cm^2 after 610 h. In comparison, our simulation of film growth at 175 mV (SOC = 0.8) yields a film resistance of 64,000 Ω-cm^2 after only 16 h. Although the system studied by Markovsky *et al.* and the one we simulated are different, the discrepancy suggests that our film conductivity is several orders of magnitude lower than that of an actual SEI. Perhaps reduction products less resistive than Li_2CO_3 make up a majority of the compact portion of the SEI. Alternatively, grain boundaries between SEI crystals may permit a less resistive pathway for lithium ions.

Gao and Macdonald[39] observed that the total resistance in their Li/solid polymer electrolyte/Li cell remained a relatively constant 16 Ω cm^2, much lower than what was obtained in our simulations. Again, this is a consequence of the wide variation in SEI products that can be formed in different lithium-metal and lithium-ion cells, compounded by our underestimation of ionic conductivity in the present study. The true film resistance is likely much smaller than 16 Ω-cm^2, since the overall cell resistance does not increase in accordance with film thickness. Indeed, Gao and Macdonald estimate that the electrolyte resistance is the dominant term in their system, and the thickness of their electrolyte layer (300 to 400 μm) is much greater than that of a typical cell.

Gao and Macdonald also emphasize the nonreactive nature of their system's impedance over a wide range of frequencies. The film modeled in the present study should also be almost purely resistive, since charge-transfer reactions are near equilibrium and the film is considered electrically neutral. Successful implementation of Poisson's equation in future simulations will allow us to compare simulations with ac impedance experiments that indicate significant capacitive components in actual lithium-ion cells.

The wide range in SEI resistance reported in the literature is a result not only of the large variation in cell chemistries and experimental conditions, but also the ambiguity of ac impedance spectra, which are most commonly employed to determine film resistance.[3,16,21,28-32,49,61-63] There is little uniformity in the equivalent circuits used to account for ac impedance results, although a series of RC circuits seems to be the most common model.[3,32]

The simulated film thicknesses given here do agree in magnitude with those reported in the literature.[13,14,23,27,28,59,60,64] To our knowledge, no direct measurement of the SEI growth rate has been made, although one could infer a film growth rate from the measured rate of capacity loss and Eq. 42, assuming the film has a particular density of lithium. Alliata *et al.*[64] and Jeong *et al.*[14] report film thickness on highly oriented pyrolytic graphite after the first and second cycles, and both studies show a significant increase in film thickness during the second cycle. Film growth was greater in the latter study (40 nm after the first cycle, 70 nm after the second), in which a slower sweep rate (0.5 mV/s) was used during cyclic voltammetry.[14] Alliata *et al.* used a faster sweep rate (5 mV/s) and observed roughly one-third the film growth after each cycle (15 nm after the first cycle, 25 nm after the second).[64] Slightly different cosolvents (DEC[14] *vs.* DMC[64]) were used in the two studies, although both contained EC and 1 M $LiClO_4$.

We have also attempted to simulate film growth with a very low electron concentration, corresponding to a bandgap of 2 to 3 eV, and with high electron mobility, assuming typical values for insulating solids.[7] In this case, we wish to vary the electron concentration over the range 10^{-30} to 10^{-10} M and the diffusion coefficient over the range 0.1 to 100 cm^2/s. With such a minuscule concentration of electrons, electroneutrality will be satisfied only if the much higher concentration of lithium interstitials is balanced by that of lithium vacancies. In this case, the concentration of both lithium species would remain relatively constant, unless electrons were injected into the film at such an enormous rate that the electron concentration increased by many orders of magnitude.

Difficulties in simulating this system stem from the fact that small errors in calculating net rates of reaction result in a nonzero flux of film species, which in turn leads to spurious changes in the electron concentration. Measures have been taken to remedy these errors and give more accurate results. For instance, the roundoff error inherent in calculating fluxes by summing migration and diffusion terms can be eliminated by introducing a new variable

$$A_k = c_k \exp\left(z_k \frac{F}{RT}\Phi\right) \quad [47]$$

so that the flux (neglecting convection, which is small) can be expressed as

$$N_k = -D_k \frac{\partial A_k}{\partial x} \exp\left(-z_k \frac{F}{RT}\Phi\right) \quad [48]$$

Although it is not formally discussed, this development is included in a computer program contained in Ref. 65.

The heterogeneous reactions can be expressed in terms of an exchange current density (i_0) and surface overpotential (η_s) as follows

$$R_{Al} = \frac{i_{0,1}}{n_1 F}\left[\exp\left(\frac{\alpha_{a,1}F}{RT}\eta_{s,1}\right) - \exp\left(-\frac{\alpha_{c,1}F}{RT}\eta_{s,1}\right)\right] \quad [49]$$

where

$$i_{0,1} = \left(k_{c,1}\prod_k^{\text{products}} c_k^{-s_{k,1}}\right)^{1-\beta_1}\left(k_{a,1}\prod_k^{\text{reactants}} c_k^{s_{k,1}}\right)^{\beta_1} \quad [50]$$

$$\eta_{s,1} = V - V_{eq,1} \quad [51]$$

$$V_{eq,1} = \frac{RT}{n_1 F}\left(\ln k_{c,1} - \ln k_{a,1} - \sum_k^{\text{all\_species}} s_{k,1}\ln c_k\right) \quad [52]$$

$$\alpha_{a,1} = n_1(1-\beta_1) \quad [53]$$

$$\alpha_{c,1} = n_1\beta_1 \quad [54]$$

When the overpotential is close to zero, there may be significant roundoff error when subtracting the cathodic portion of the reaction from the anodic portion. In these instances, an expanded form of Eq. 49, valid for small overpotentials, may be more suitable[66]

$$R_{Al} = \frac{i_{0,1}}{n_1 F}\left[(\alpha_{a,1}+\alpha_{c,1})\frac{F\eta_{s,1}}{RT} + \frac{\alpha_{a,1}^2 - \alpha_{c,1}^2}{2}\left(\frac{F\eta_{s,1}}{RT}\right)^2 + \frac{\alpha_{a,1}^3 + \alpha_{c,1}^3}{6}\left(\frac{F\eta_{s,1}}{RT}\right)^3 + O(\eta_{s,1}^4)\right] \quad [55]$$

Note that the second even-powered terms will cancel if $\beta_1 = 1/2$. In some cases, for very fast kinetics (high exchange current density), an equilibrium expression may be assumed, although this eliminates a degree of freedom, and the overall mass balance of a particular

species may not be maintained rigorously. However, for a minor species such as electrons in the film, this may not be a substantial sacrifice.

Conclusions

Several parameters are critical in estimating not only the film-growth characteristics, but also the growth-law regime that characterizes our system. These parameters include physical properties of the film (electronic and ionic mobilities), characteristics of the electrode/film/electrolyte system (heterogeneous kinetic and equilibrium constants), physical parameters set by the experimentalist or battery manufacturer (graphite particle size), and operating conditions (SOC).

Although the simulated film thickness generally agreed with experimental measurements, the simulated film resistance was several orders of magnitude higher than that which has been determined experimentally. Likewise, the ratio of normalized *ICL* to film thickness for Li_2CO_3 used in the model was higher than the ratio of experimentally determined *ICL* to observed SEI thickness in experimental cells. These discrepancies support the idea of a complex multilayer SEI containing high-molecular-weight products (including polymers) in the outer layer and less resistive products in the compact inner layer. Another explanation for the low experimentally measured film resistance could be alternative modes of ionic transport (*e.g.*, via grain boundaries). Direct comparison of our model predictions with experimental measurements may be more meaningful for a system in which Li_2CO_3 is the primary film component.

Irreversible capacity loss and film resistance are crucial factors in the design of a successful lithium-ion battery, and our model predicts that film growth affects both of these values. While film growth on large 10 μm particles does not account for significant irreversible capacity loss, it does increase the resistance of the system, and therefore can lead to power loss. The trade-off between low capacity and ohmic losses for large particles and increased reaction surface for small particles implies a particle-size optimum.

Acknowledgments

This work was supported by the Assistant Secretary for Energy Efficiency and Renewable Energy, Office of FreedomCAR and Vehicle Technologies of the U.S. Department of Energy under Contract No. DE-AC03-76SF00098, and by the National Science Foundation.

University of California, Berkeley, assisted in meeting the publication costs of this article.

List of Symbols

c_k	concentration of species k, mol/m^3
D_k	diffusion coefficient of species k, cm^2/s
D_S	diffusion coefficient of Li in the electrode material, cm^2/s
F	Faraday's constant, 96,487 C/mol
i	current density, A/m^2
i_0	exchange current density, A/m^2
k_a	anodic rate constant (various units)
k_c	cathodic rate constant (various units)
K	equilibrium constant (various units)
K_{global}	overall intercalation/deintercalation equilibrium constant
L	film thickness, porous electrode thickness, m
M_k	molecular symbol for species k
m	film-growth order
n	number of electrons transferred
N_k	molar flux of species k, mol/cm^2-s
R	gas constant = 8.314 J/mol-K
R_{Al}	rate of heterogeneous reaction 1, mol/cm^2-s
R_1	rate of homogeneous reaction 1, mol/cm^2-s
$s_{k,1}$	stoichiometric coefficient of species k in reaction 1
t	time, s
t_k^0	transference number of species k, referenced to the lattice
T	temperature, K
v_I	velocity of film/solution interface, m/s
v_L	lattice velocity, m/s
V	potential difference across interface, V
V_{eq}	equilibrium potential, V
x	spatial coordinate, m
x_{Li}	state of charge in graphite
z	charge number

Greek

α	phase to the left of the interface
α_a	anodic transfer coefficient
α_c	cathodic transfer coefficient
β	symmetry factor
γ	phase to the right of the interface
Γ	concentration of adsorbed species, mol/m^2
δ_1	distance between film OHP and solution IHP
δ_2	distance between solution IHP and OHP
ε	electric permittivity C/V-m
ε_0	electric permittivity of free space, 8.85×10^{-12} C/V-m
η_s	surface overpotential, V
λ	Debye length, m
μ, ν	material balance coefficients
ρ	density, g/cm^3
σ	electric conductivity, S/cm
ξ	dimensionless distance from electrode/film interface

Subscripts

film	in the film
k	species index
1	reaction index
Li	property of lithium in the electrode
sol	in the solution

Film species

e^-	electron
h^+	hole
Li_i^+	lithium interstitial
Li_{Li}	filled lithium site
V_{Li}^-	lithium vacancy

References

1. *Review of the Research Program of the Partnership for a New Generation of Vehicles: Seventh Report*, National Academy Press, Washington, DC (2001).
2. D. Aurbach, in *Advances in Lithium-Ion Batteries*, W. A. v. Schalkwijk and B. Scrosati, Editors, p. 7, Academic/Plenem Publishers, New York (2002).
3. D. Aurbach, B. Markovsky, I. Weissman, E. Levi, and Y. Ein-Eli, *Electrochim. Acta*, **45**, 67 (1999).
4. D. N. Bennion and E. L. Littauer, *J. Electrochem. Soc.*, **123**, 1462 (1976).
5. E. Peled, *J. Electrochem. Soc.*, **126**, 2047 (1979).
6. E. Peled, in *Lithium Batteries*, J.-P. Gabano, Editor, p. 43, Academic Press, London (1983).
7. J. Newman, *Electrochemical Systems*, 2nd ed., Prentice Hall, Englewood Cliffs, NJ (1991).
8. V. Battaglia and J. Newman, *J. Electrochem. Soc.*, **142**, 1423 (1995).
9. D. D. Macdonald, S. R. Biaggio, and H. K. Song, *J. Electrochem. Soc.*, **139**, 170 (1992).
10. D. Aurbach, M. L. Daroux, P. W. Faguy, and E. Yeager, *J. Electrochem. Soc.*, **134**, 1611 (1987).
11. D. Bar-Tow, E. Peled, and L. Burstein, *J. Electrochem. Soc.*, **146**, 824 (1999).
12. D. Aurbach, Y. Ein-Ely, and A. Zaban, *J. Electrochem. Soc.*, **141**, L1 (1994).
13. A. M. Andersson, A. Henningson, H. Siegbahn, U. Jansson, and K. Edström, *J. Power Sources*, **119**, 522 (2003).
14. S. K. Jeong, M. Inaba, T. Abe, and Z. Ogumi, *J. Electrochem. Soc.*, **148**, A989 (2001).
15. D. P. Abraham, J. Liu, C. H. Chen, Y. E. Hyung, M. Stoll, N. Elsen, S. MacLaren, R. Twesten, R. Haasch, E. Sammann, I. Petrov, K. Amine, and G. Henriksen, *J. Power Sources*, **119**, 511 (2003).
16. E. Peled, D. Golodnitsky, and G. Ardel, *J. Electrochem. Soc.*, **144**, L208 (1997).
17. M. Wachtler, J. O. Besenhard, and M. Winter, *J. Power Sources*, **94**, 189 (2001).
18. M. Winter and J. O. Besenhard, *Electrochim. Acta*, **45**, 31 (1999).
19. P. Arora, R. E. White, and M. Doyle, *J. Electrochem. Soc.*, **145**, 3647 (1998).
20. E. Wang, D. Ofer, W. Bowden, N. Iltchev, R. Moses, and K. Brandt, *J. Electrochem. Soc.*, **147**, 4023 (2000).
21. D. Aurbach, B. Markovsky, M. D. Levi, E. Levi, A. Schechter, M. Moshkovich, and Y. Cohen, *J. Power Sources*, **82**, 95 (1999).
22. S. E. Sloop, J. B. Kerr, and K. Kinoshita, *J. Power Sources*, **119**, 330 (2003).
23. S. K. Jeong, M. Inaba, Y. Iriyama, T. Abe, and Z. Ogumi, *Electrochim. Acta*, **47**, 1975 (2002).
24. K. Kinoshita, in *Energy Storage Systems for Electronics*, T. Osaka and M. Datta, Editors, p. 193, Gordon and Breach Publishers, Langhorne, PA (2000).
25. K. C. Tsaur and R. Pollard, *J. Electrochem. Soc.*, **131**, 975 (1984).
26. K. C. Tsaur and R. Pollard, *J. Electrochem. Soc.*, **131**, 984 (1984).
27. A. V. Churikov, E. S. Nimon, and A. L. L'vov, *Russ. J. Electrochem.*, **34**, 591 (1998).
28. A. V. Churikov, I. M. Gamayunova, and A. V. Shirokov, *J. Solid State Electrochem.*, **4**, 216 (2000).
29. J. G. Thevenin and R. H. Muller, *J. Electrochem. Soc.*, **134**, 273 (1987).
30. N. R. Avery and K. J. Black, *J. Power Sources*, **68**, 191 (1997).

31. A. V. Churikov and A. L. L'vov, *Russ. J. Electrochem.*, **34**, 584 (1998).
32. C. S. Wang, A. J. Appleby, and F. E. Little, *J. Electroanal. Chem.*, **497**, 33 (2001).
33. V. S. Battaglia, Ph.D. Thesis, University of California, Berkeley, Berkeley, CA (1993).
34. E. J. W. Verway, *Physica (Amsterdam)*, **2**, 1059 (1935).
35. C. Y. Chao, L. F. Lin, and D. D. Macdonald, *J. Electrochem. Soc.*, **128**, 1187 (1981).
36. F. P. Fehlner and N. F. Mott, *Oxidation of Metals* , **2**, 59 (1970).
37. K. J. Vetter and F. Gorn, *Electrochim. Acta*, **18**, 321 (1973).
38. N. Cabrera and N. F. Mott, *Rep. Prog. Phys.*, **12**, 163 (1948).
39. L. Gao and D. D. Macdonald, *J. Electrochem. Soc.*, **144**, 1174 (1997).
40. R. J. Maurer, *J. Chem. Phys.*, **9**, 579 (1941).
41. J. Mizusaki, H. Tagawa, K. Saito, K. Uchida, and M. Tezuka, *Solid State Ionics*, **53-6**, 791 (1992).
42. J. M. Tarascon and D. Guyomard, *Solid State Ionics*, **69**, 293 (1994).
43. C. M. Doyle, Ph.D. Thesis, University of California, Berkeley, Berkeley, CA (1995).
44. K. E. Thomas, Ph.D. Thesis, University of California, Berkeley, Berkeley, CA (2002).
45. D. Guyomard and J. M. Tarascon, *J. Electrochem. Soc.*, **139**, 937 (1992).
46. R. H. Perry and D. W. Green, *Perry's Chemical Engineer's Handbook*, pp. 2-17, McGraw Hill, New York (1997).
47. J. A. Riddick, W. B. Bunger, and T. K. Sakano, *Organic Solvents: Physical Properties and Methods of Purification*, p. 433, Wiley-Interscience, New York (1986).
48. J. Shim and K. A. Striebel, *J. Power Sources*, **119**, 934 (2003).
49. K. Zaghib, X. Song, A. Guerfi, R. Rioux, and K. Kinoshita, *J. Power Sources*, **119**, 8 (2003).
50. G. Ning, B. Haran, and B. N. Popov, *J. Power Sources*, **117**, 160 (2003).
51. F. Cao, I. V. Barsukov, H. J. Bang, P. Zaleski, and J. Prakash, *J. Electrochem. Soc.*, **147**, 3579 (2000).
52. S. S. Zhang, M. S. Ding, K. Xu, J. Allen, and T. R. Jow, *Electrochem. Solid-State Lett.*, **4**, A206 (2001).
53. J. Vetter and P. Novák, *J. Power Sources*, **119**, 338 (2003).
54. K. C. Möller, H. J. Santner, W. Kern, S. Yamaguchi, J. O. Besenhard, and M. Winter, *J. Power Sources*, **119**, 561 (2003).
55. J. Christensen and J. Newman, *J. Electrochem. Soc.*, **150**, A1416 (2003).
56. K. Zaghib, G. Nadeau, and K. Kinoshita, *J. Electrochem. Soc.*, **147**, 2110 (2000).
57. P. Yu, J. A. Ritter, R. E. White, and B. N. Popov, *J. Electrochem. Soc.*, **147**, 1280 (2000).
58. D. Aurbach, H. Teller, M. Koltypin, and E. Levi, *J. Power Sources*, **119**, 2 (2003).
59. M. Inaba, Y. Kawatate, A. Funabiki, S. K. Jeong, T. Abe, and Z. Ogumi, *Electrochim. Acta*, **45**, 99 (1999).
60. S. K. Jeong, M. Inaba, R. Mogi, Y. Iriyama, T. Abe, and Z. Ogumi, *Langmuir*, **17**, 8281 (2001).
61. B. Markovsky, A. Rodkin, Y. S. Cohen, O. Palchik, E. Levi, D. Aurbach, H.-J. Kim, and M. Schmidt, *J. Power Sources*, **119**, 504 (2003).
62. C. S. Wang, I. Kakwan, A. J. Appleby, and F. E. Little, *J. Electroanal. Chem.*, **489**, 55 (2000).
63. J. S. Gnanaraj, E. Zinigrad, M. D. Levi, D. Aurbach, and M. Schmidt, *J. Power Sources*, **119**, 799 (2003).
64. D. Alliata, R. Kotz, P. Novák, and H. Siegenthaler, *Electrochem. Commun.*, **2**, 436 (2000).
65. M. E. Orazem, Ph.D. Thesis, University of California, Berkeley, Berkeley, CA (1983).
66. R. Pollard, Ph.D. Thesis, University of California, Berkeley, Berkeley, CA (1980).